Terr. Atmos. Ocean. Sci., Vol. 30, No. 2, 171-184, April 2019 doi: 10.3319/TAO.2018.12.04.01

NTU/PU model simulations and observed flow over mountains

Patrick Haines[1, *], Wen-Yih Sun[2, 3], Shu-Hua Chen[4], Wu-Ron Hsu[5], and Ming-En Hsieh[6]

[1] *U.S. Army Research Laboratory, White Sands Missile Range, NM*
[2] *Department of Earth, Atmospheric, and Planetary Sciences, Purdue University, USA*
[3] *Department of Atmospheric Sciences, National Central University, Taoyuan City, Taiwan*
[4] *Department of Land, Air and Water Resources, University of California, Davis, USA*
[5] *Retired, Department of Atmospheric Sciences, National Taiwan University, Taipei City, Taiwan*
[6] *Taiwan Typhoon and Flood Research Institute, Taipei City, Taiwan*

Article history:
Received 12 September 2017
Revised 30 November 2018
Accepted 4 December 2018

Keywords:
Nonhydrostatic model, Compressible, Forward-backward, Lee-vortex, Hydraulic jump, Mountain waves

Citation:
Haines, P., W.-Y. Sun, S.-H. Chen, W.-R. Hsu, and M.-E. Hsieh, 2019: NTU/PU model simulations and observed flow over mountains. Terr. Atmos. Ocean. Sci., 30, 171-184, doi: 10.3319/TAO.2018.12.04.01

ABSTRACT

The National Taiwan University/Purdue (NTU/PU) nonhydrostatic model is used to study mountain waves, hydraulic jumps, and lee vortices. The NTU/PU model is based on a compressible and three-dimensional system of equations with a terrain-following vertical coordinate. A major advantage of the model is the use of a modified forward-backward integration scheme that retains internal gravity waves but suppresses unwanted sound waves. In flow around an isolated ideal elliptical mountain, the simulated flow from the NTU/PU model spreads broadly in the crosswind direction with a well-defined stagnation point at the windward side of the mountain. Two semi-idealized downslope wind cases were conducted using the real topography at White Sand Missile Range (WSMR), New Mexico, USA. Our simulated flows including hydraulic jumps and vortex shedding in the lee of the Organ Mountains agree very well with observations for the case on 25 January 2004, at 15 UTC, but the discrepancy is somewhat larger for the case on 19 January 2004, at 15 UTC. This paper shows that the model results are sensitive to the detailed numerical schemes, filters, and physics, etc. It also suggests that more observations and improvements are required for a model to realistically simulate the flow over complex terrain.

1. INTRODUCTION

Studies of airflow are often complicated by the wide range of horizontal scales of motion that must be considered. For example, to properly simulate large-scale weather systems, a large computation domain must be used, and at the same time high spatial resolution is needed in order to resolve motions with smaller scales. Thus, meteorological modeling can be a very demanding problem in terms of computing resources. This is especially the case for airflow over mountains. In addition to the complicated length scales over complex terrain, several natural length scales of atmospheric systems are also important, such as the variation of stratification and wind in space, the thickness of the atmospheric boundary layer, the distance of downwind drift during a buoyancy oscillation, the distance associated with the inertial oscillation, the formation and propagation of lee-vortices and hydraulic jump, etc. (Smith 1979). It is also noted that lee vortices, hydraulic jumps, and lee waves simulated from a free-slip surface can be quite different than those from a viscous surface (Sun and Hsu 2005), but it is also difficult to find an appropriate surface friction and roughness over mountains.

Developing a capability to predict wind flows in and around complex terrain is important to the US. Army as well as to aviation and many other civilian activities. Such a capability ought to apply to both high wind phenomena such as strong downslope wind flows, lee waves, and hydraulic jumps and low wind situations in which very complex flows are often seen. Several observational programs have been conducted for high wind events (e.g., Mobbs et al. 2005; Sheridan et al. 2007; Grubišić et al. 2008) while several other programs have been done for light wind complex flow environments (e.g., Whiteman et al. 2008; Fernando et al. 2015, 2018). Because these programs are by necessity of limited time extent, they may not fully sample the wide variety and extrema of possible complex terrain flow situations.

* *Corresponding author*
E-mail: patrick.a.haines6.civ@mail.mil

White Sands Missile Range (WSMR) located in southern New Mexico is a US Army testing area covering almost 3200 square miles. WSMR conducts year round tests of missile and other systems for the US military and foreign countries. In support of these test activities, WSMR operates a network of about 30 instrumented 10 m meteorological towers which is distributed over the entire WSMR test range; a few of the towers are located external to WSMR in nearby areas. This network is called the Surface Atmosphere Measurement System (SAMS) and it produces 5 minute average (15 minute averages prior to 2010) surface meteorological values at the standard measurement levels.

WSMR headquarters (HQ) is located in the southwestern part of WSMR lies about 5 - 8 km north and east of a very steep mountain range that rises as much as 1500 m above it. During late winter and spring, fairly frequent downslope wind events occur there and sometimes these include lee waves and even rotor flow. A recent WSMR in-house study found that, on average, there are 7 or more events in which the average surface wind at the WSMR HQ SAMS site exceeds 50 knots for at least 15 minutes (Thomas 2014). These high wind events are concentrated in the February through April time period when there are many additional windy days in which the average wind speed, although high, does not exceed 50 knots for at least 15 minutes. Maximum winds for shorter time periods and gusts can be substantially higher. Throughout the year when winds are low and especially at night, the wind flow in and near these mountains is often very complex. Besides presenting considerable predictability challenges to numerical weather prediction (NWP), the complexity of these events is generally not completely shown in the SAMS data because the spacing of the SAMS sites is not sufficiently dense. However, in 2004, five fully instrumented 10 m Army Research Laboratory (ARL) MET towers were collocated with the four SAMS' sites close to WSMR HQ. Thus, there was a fairly dense network operating for an extended period then. In addition to the MET towers, there was a Wind Profiling radar located downwind of the mountains and a Remote Automatic Weather Stations (RAWS) surface MET station located on the windward side of the mountains.

During 2004, there was a notable downwind lee wave event and several very complex low wind flow situations. The National Taiwan University/Purdue University (NTU/PU) nonhydrostatic model (Hsu and Sun 2001) is used to study mountain waves, hydraulic jumps, lee waves and complex wind flow such as vortices. This model is based on a compressible three-dimensional system of equations with a terrain-following vertical coordinate. The model employs a modified forward-backward integration scheme that retains internal gravity waves but suppresses unwanted sound waves. In flow around an isolated ideal elliptical mountain, the simulated flow from the NTU/PU model spreads broadly in the crosswind direction with a well-defined stagnation point at the windward side of the mountain. Two semi-idealized downslope wind cases were conducted using the real topography at White Sand Missile Range (WSMR), New Mexico, USA. We would like find out whether the observed phenomena can be simulated by the model with a resolution of order of 1 km, which may not be good enough to fully resolve the detail of the terrain but is much better than current operational models. If the model can reproduce the observations, then, we would like to understand the dynamics responsible for these phenomena as well as how to improve the physics, mathematics, and numerical schemes of the model. Our simulated flows including hydraulic jumps, lee waves and vortex shedding in the lee of the Organ Mountains agree very well with observations for the case on 25 January 2004, at 15 UTC, but the discrepancy is somewhat larger for the case on 19 January 2004, at 15 UTC. This paper shows that the model results are sensitive to the detailed numerical scheme, filter, and physics, etc. It also suggests that more observations and improvements are required for a model to realistically simulate the flow over complex terrain.

In section 2, we include a brief description of the numerical model used along with several references, which contain more detailed descriptions and background about the model's numerical and physical basis. In section 3, we show and discuss the modelled results for flow over and around an idealized elliptical terrain obstacle. In section 4, we show the model simulations for the two real cases and discuss the comparisons between the model results and the observations; we also show the results for a uniform 5 m s^{-1} westerly flow impinging on the mountains. Finally, the conclusions of this paper are given in section 5. In comparison to the observations, the current model has very good performance.

2. NUMERICAL MODEL

The NTU/PU Nonhydrostatic Numerical Model (Hsu and Sun 2001; Sun and Hsu 2005) is used in this study. The model solves a three-dimensional, compressible, and nonhydrostatic system of equation with a terrain-following vertical coordinate (Haines et al. 1997; Chen and Sun 2001). The model is a semi-implicit model in terms of the time-integration scheme. The algorithm is stable and does not generate computational modes as shown in Hsu and Sun (2001) and Sun (2011). In addition, using a time-splitting scheme and parallel computing (Hsu et al. 2006; Shieh et al. 2006, 2011), we also modify the 3D divergence equation as discussed in Sun et al. (2012, 2013) to suppress unwanted high-frequency sound waves while not damping internal gravity waves in order to increase the time step according to the CFL criterion.

We followed the work of Deardorff (1980) and Sun and Chang (1986) for the turbulence scheme with the exception that all spatial derivatives are corrected for the terrain following coordinate. An implicit scheme is used to calculate

Earth's rotational effect. As for the treatment of surface friction, the similarity equations were applied. The basic equations and the original forward-backward schemes can be found in Hsu and Sun (2001). The semi-implicit scheme developed by Sun (2011) is applied to solve the terms involved in the various wave phenomena, and the advection scheme in Sun (1993) is used to solve the advection terms. Comparisons between the filtered acoustic waves by using the implicit vertical scheme and the modified 3D divergence equation applied in the NTU/PU model was discussed in Sun et al. (2012, 2013). In addition to its basic dynamic framework, the model takes into account many physical processes, such as land/ocean processes, cloud microphysics, atmospheric turbulence, etc., that are also included in the Purdue Regional Climate Model (Sun et al. 2008).

3. FLOW OVER AN IDEALIZED MOUNTAIN

Although the simulation of a 2D bell-shaped mountain generated by the NTU/PU model is comparable to the other models' output (Doyle et al. 2000), it is important to see whether the model can handle the circulation moving around and over a 3D mountain, including the separation of flow and the stagnation at the inflow region, the vortex-shedding, wake, and hydraulic jump on the lee side, as well as the gravity waves and shock waves. Furthermore, the idealized case is easy to compare with other theoretical results and numerical simulations (Hunt et al. 1988; Chern 1989; Smith and Grønås 1993). It is also noted that results generated from a circular mountain produces a pair of vortices on the lee side instead of vortex shedding because of symmetric forces generated by the mountain (Sun and Chern 1994). The NTU/PU model is applied to simulate the flow over an idealized elliptical bell-shaped mountain with a top at z = 2 km; the half-width lengths are 10 and 5 km in the long and short horizontal axis directions, respectively, and the major axis is tilted by 30 degrees clockwise from the north. The incoming westerly wind is a uniform 4 m s^{-1} with a constant stratification of $N^2 = 10^{-4}$ s^{-2} over a free-slip surface. Hence, the Froude number is Fr = U/Nh = 0.2 for this flow, although the Froude number derived from a 2D mountain based on the Boussinesq fluid is an inappropriate parameter for the air flow moving over a 3D mountain. Further discussion will be presented later or is referred to Sun and Sun (2015). The domain consists of (600, 300, 50) grids in the (x, y, z) directions respectively with $\Delta x = \Delta y = 1$ km and $\Delta z = 300$ m.

The numerical simulations at 10 and 20 hr integrations from the model are shown in Figs. 1 and 2, respectively. Overall, the flow pattern after 10 hr-integration is similar and comparable with the simulations shown in Chern (1989) and Sun and Chern (1994), with a tilt elliptical mountain. It is noticed that the stagnation point is well-defined in this simulation. The vortex shedding after 20 hr-integration is shown in Fig. 2. We can see that both cyclonic and anti-cyclonic circulations in Fig. 1 move downstream with little dispersion. Meanwhile, a new anti-circulation forms near the mountain. They are similar to the vortex shedding discussed in Sun and Chern (1994). In addition to the unsymmetrical force created by the tilting mountain, generation of lee vortex or vortex shedding from a 3D mountain also requires friction

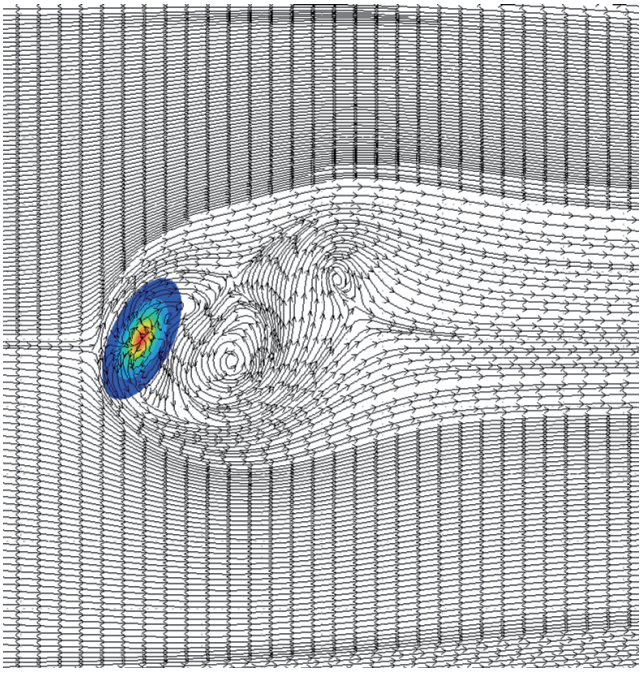

Fig. 1. NTU/PU simulated surface streamline after 10-hr integration.

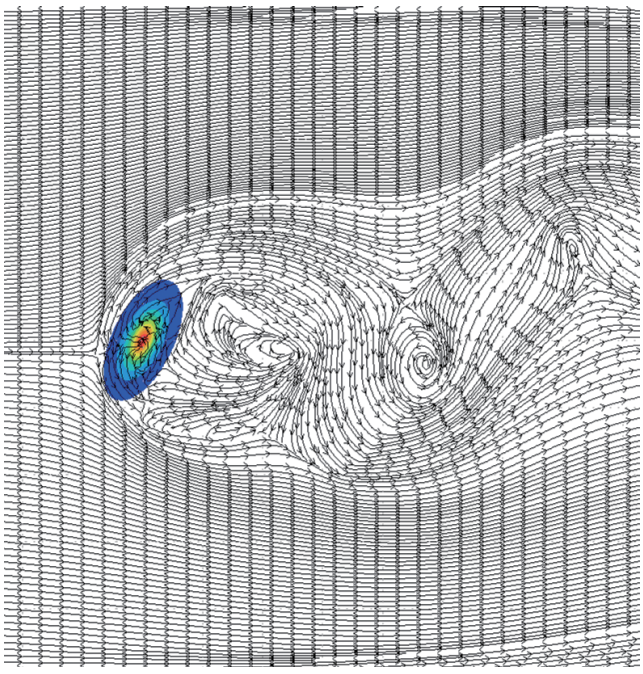

Fig. 2. NTU/PU simulated surface streamline after 20-hr integration.

and vertical stretching in the vorticity equation (Sun et al. 1991; Sun 2016). Hence, they are quite different from the 2D vortex shedding generated from a cylinder due to high Reynolds number without vertical stretching as shown in Wen and Lin (2001), although the patterns look quite similar to each other.

4. NUMERICAL SIMULATIONS OVER WHITE SANDS MISSILE RANGE

Numerous observational and modeling studies have revealed a wide variety of flows around and above terrain obstacles. Most such studies, however, have considered fairly simple terrain such as an isolated summit (Sun and Chern 1994) or a long barrier perpendicular to an impinging flow (Doyle et al. 2000; Chen and Sun 2001; Sun and Sun 2013, 2015). Real terrain and real atmospheric conditions are more complex than those used in the previously mentioned studies and the resulting phenomena are more complicated and diverse.

WSMR lies to the lee of the Organ and San Andres Mountains in the Tularosa Basin in southern New Mexico. The Organ mountain massif is a rugged quasi-circular 1500-m high obstacle with a diameter of about 10 km and peak of 2704 m above sea level (asl). It is connected to a narrow and remarkably steep 1 - 1.5 km wide SSE-NNW oriented ridge to its north. That ridge, in turn, is connected to the approximately 100-km long south to north oriented barrier of the San Andres Mountains. Several passes and one massif complicate the San Andres barrier. Because of the terrain variety, for a given situation at WSMR, it is possible to have both sub-critical and super-critical flow in fairly close proximity greatly complicating the resulting flow and presenting significant challenges to numerical models (Haines et al. 2003, 2006).

4.1 WSMR Observations

From early January to March 2004, ARL set up five fully instrumented 10 m towers in the lee of the Organ Mountains. Each tower measured and recorded the wind direction and wind speed at a height of 10 m above ground level, as well as pressure, humidity, and temperature at a height of 2 m above ground level. Of special interest was the fact that the pressure instruments were quite accurate and calibrated establishing an accuracy of +/- 10 pascals or better. Meanwhile, ARL also collected data from several of the nearby WSMR SAMS stations as well as RAWS in the vicinity of WSMR. The SAMS pressure sensors are annually calibrated to an accuracy of +/- 50 pascals. Altogether there were 8 stations within an approximately 20 × 25 km region at and around WSMR Headquarters affording a fairly detailed look at the complexity of the wind flow in and in proximity to the terrain. Six of the stations were located within an approximately 5 × 5 km region just to the east of the terrain enabling a highly detailed look at the pressure perturbations associated with a downslope wind event. Four of these stations were the ARL towers and two were SAMS. During the observation period, there were several downslope wind storms and a variety of blocked-flow episodes. Besides the collected surface data, we obtained the vertical and horizontal wind profiles recorded by the wind profiling radar at WSMR that is situated about 15 - 20 km downwind of the mountains. This radar system provides data coverage from about 500 m above its ground elevation (4000 feet) to about 17 km asl.

4.2 Lee Waves/ Hydraulic Jump on 25 January 2004

On 25 January 2004, a downslope wind storm occurred along the lee of the Organ and San Andres Mountains; it included formation of a train of lee waves that extended downwind across the Tularosa Basin and a hydraulic jump just to the lee of the mountains that was well-observed by the ARL and WSMR SAMS stations. These storms occur occasionally at White Sands, but this day's storm is especially noteworthy because the surface and other observations are able to document many of its facets and provide detailed comparisons to the numerical model results (Haines et al. 2006).

To simulate this case, the NTU/PU model was set up with a vertical grid spacing of 300 m, and a horizontal resolution of 1 km. DTED level 1 terrain data was used to bi-linearly interpolate the approximately 30 m resolution DTED terrain data onto a 201 × 201 km grid centered just to the east of the San Augustine Pass. After the initial terrain field was smoothed to eliminate two-delta waves and at the model domain's periphery, the model's maximum terrain heights were somewhat less than the actual terrain. By experimenting, we found that by treating the terrain with a two-step process, we could obtain maximum terrain heights quite close to the actual values (Takacs 1985). In the first step, the difference between the initial terrain height and 1400 m asl for points above 1400 m was multiplied by 1.4. Then, in the second step, the resulting combination of adjusted and unadjusted terrain heights was smoothed. Of course, it was not possible to obtain the maximum height of very narrow features such as the Organ Mountains ridge, but as can be seen in Fig. 3 the maximum height of the Organ Mountains (2720 m) and of the southern massif of the San Andres Mountains (2189 m) are well replicated in the terrain field used in this study. At the same time, the horizontal breadths of the mountains and the height of the Tularosa basin to the east of the Organ Mountains are preserved and agree extremely well with the real terrain.

Beginning with uniform application of the initial condition of the El Paso, Texas, sounding for 1200 UTC on 25 January 2004, shown in Fig. 4, the model was integrated for 4 hr or longer. Note the strong inversion in Fig. 4 at about

600 hPa or about 4000 m agl height. As shown in this figure, we calculated the Scorer parameter below and above this inversion. The Scorer Parameter is

$$l^2 = \frac{N^2}{U^2} - \frac{1}{U}\frac{d^2U}{dz^2} \quad (1)$$

(Durran 2003) where N is the Brunt-Väisälä frequency, $N = \sqrt{\frac{gd\theta}{\theta dz}}$, and $U = U(z)$ is the horizontal wind vertical profile. l, the square root of the parameter, has units of wavenumber. It is known that a significant decrease of the Scorer parameter vertically especially suddenly when gravity waves are present should result in trapped lee waves downstream from the terrain [American Meteorological Society (AMS) Glossary, http://glossary.ametsoc.org/wiki/Scorer_parameter]. The model results and observations all strongly support this. N and $\frac{d^2U}{dz^2}$ were computed as:

$$N = \sqrt{\frac{gd\theta}{\theta dz}} \quad (2)$$

$$\frac{d^2U}{dz^2} \cong \frac{U_T - 2U_M + U_B}{(\Delta z)^2} \quad (3)$$

using the 12 UTC 25 January 2004 El Paso sounding data where U_T, U_M, and U_B are the wind speed at respectively the top, middle and bottom of the two layers, and Δz is the vertical thickness of the upper and lower layers which for convenience are here taken as equal. The $d\theta/dz$ term in N was computed similarly.

"*In practice, the Scorer parameter is derived from vertical sounding profiles of wind and temperature upstream of a mountain chain to forecast the probability of trapped lee wave development. In cases where the wind data has high vertical resolution, the second term on the right-hand side of the above equation (velocity-profile curvature term) can show values of similar magnitude as the first term. This again leads to a noisy profile of the Scorer parameter. Therefore, either the wind profile is smoothed before calculating the Scorer parameter or the second term is omitted. This is acceptable since Richard S. Scorer postulated an undisturbed air flow upstream of the mountain chain as prerequisite for his parameter.*" (http://www.eumetrain.org/data/4/452/navmenu.php?tab=4&page=5.0.0)

Fortunately, the El Paso sounding is situated upstream from the Organ Mountains for the WSW flow of this case and there are no close (> 140 km) terrain features upstream of it.

The model results at 3 - 4 hr (i.e., at 0800 - 0900 local time) will be discussed here. Simulations were done for a no-slip surface (without the Coriolis force and are presented in Figs. 5 - 8). Figure 5 shows the model wind field and observations at 1500 UTC on 25 January 2004. The wind

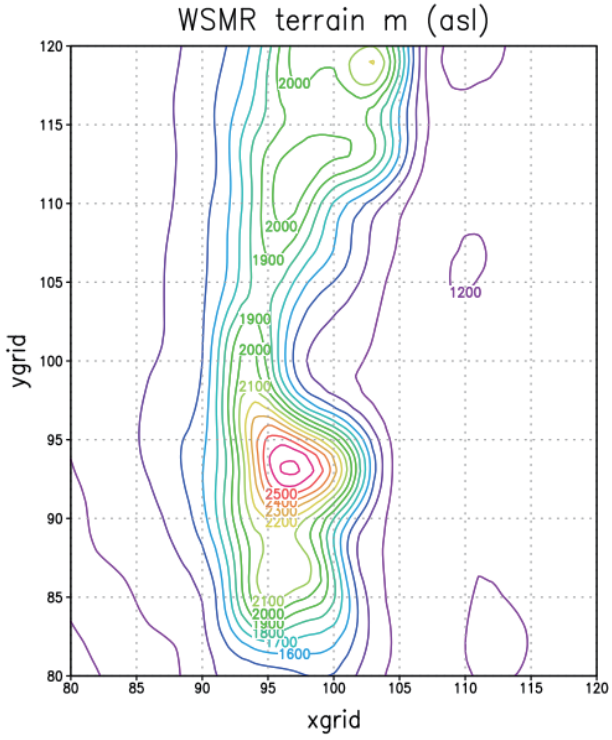

Fig. 3. Terrain used in the simulations, terrain heights are in meters above sea level and contours are at every 100 m.

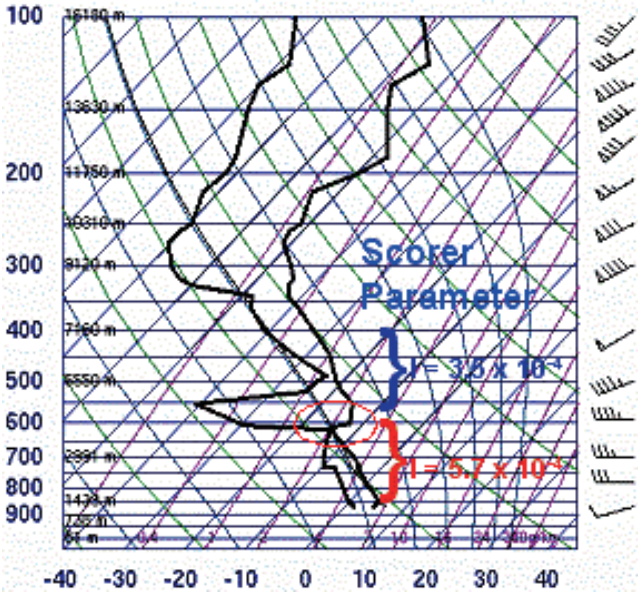

Fig. 4. El Paso, TX, sounding for 25 January 2004, at 12 UTC. Note the inversion at about the 600 hPa level. The Scorer Parameter values above and below the inversion are also shown.

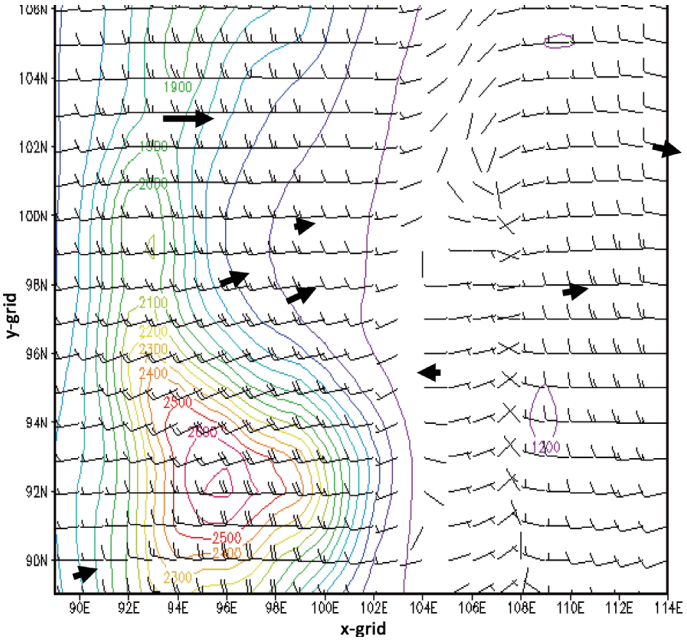

Fig. 5. Numerical simulation of 25 January downslope wind storm case at WSMR over a no-slip surface without Coriolis force at 32°N after 3-hr integration with a mountain height of 1.5 km. The vertical grid interval is 300 m and horizontal grid space is 1 km. The x-component wind is shown and the hydraulic jump remains stationary.

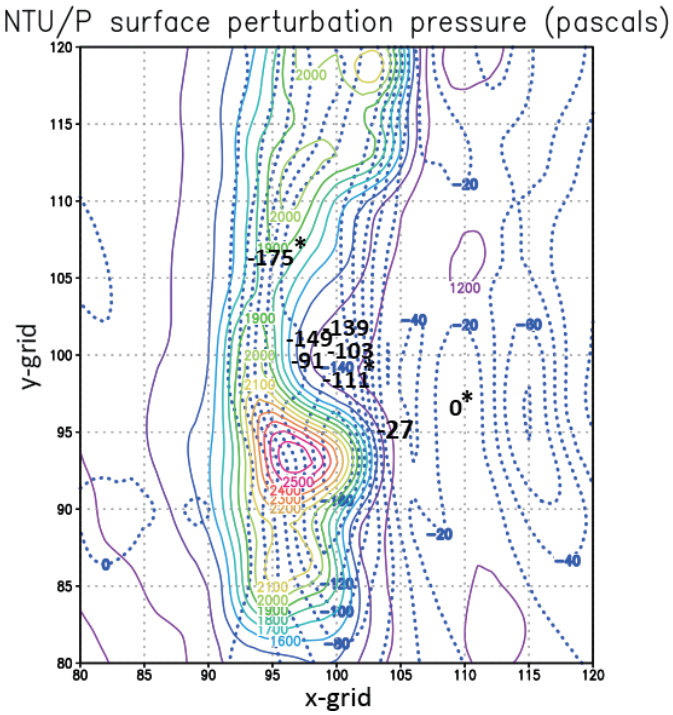

Fig. 6. Numerical simulation of 25 January downslope wind storm case at WSMR. This figure shows the NTU/PU surface pressure perturbation (pascals) field at 1500 UTC 25 January 2004. The ARL and SAMS analyzed pressure perturbations (pascals) for the same time are shown by bold numbers.

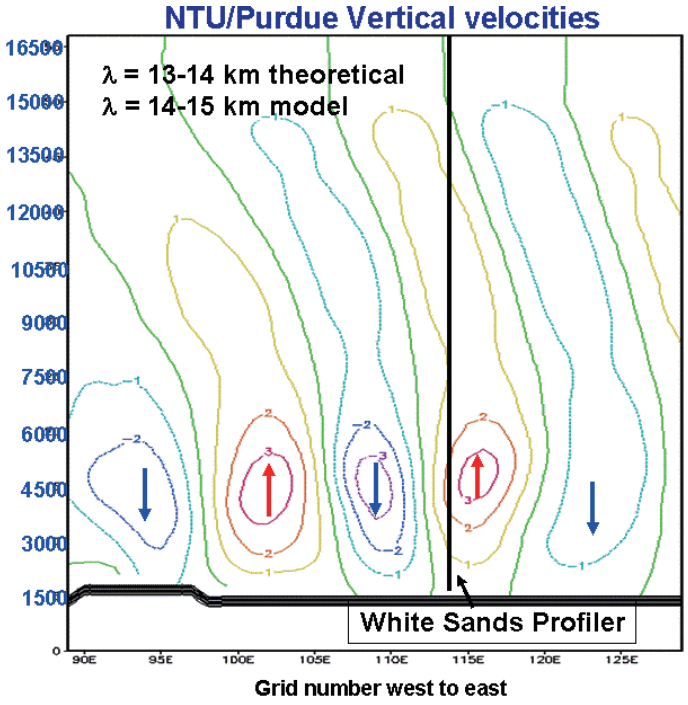

Fig. 7. NTU/PU vertical velocity (m s^{-1}) at 1500 UTC 25 January 2004, along a west to east cross section that intersects with the WSMR wind profiling radar.

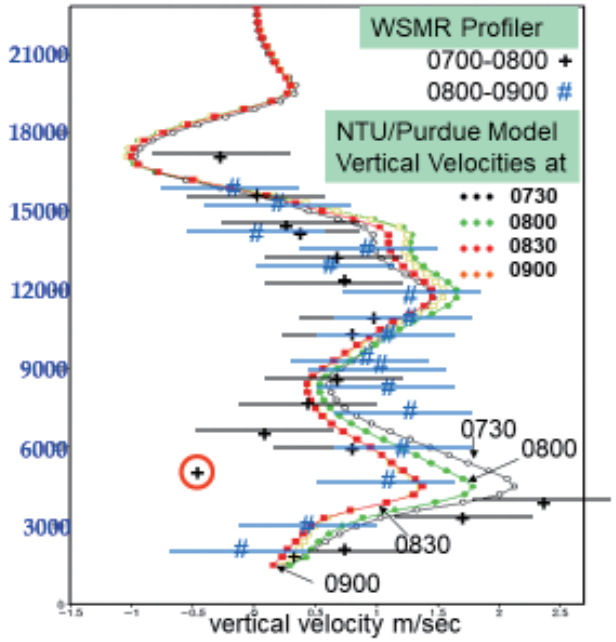

Fig. 8. NTU/PU simulated vertical velocities (m s^{-1}) from 0730 - 0900 (1430 - 1600 UTC) at the WSMR wind profiling radar location on 25 January 2004, compared to the observed WSMR wind profiling radar vertical velocities.

barbs are the NTU/PU model's surface wind field and show strong downslope flow on the lee side of the Organ and San Andres Mountains. In a band oriented south to north just east of the mountains the model's westerly surface winds abruptly weaken and then reverse (from W to E), this corresponds to the strong reverse pressure gradient shown by the pressure perturbations in Fig. 6. The transition to reversed flow is more abrupt to the lee of the higher terrain such as the Organ Mountains and the higher terrain to the north of WSMR's main post. The reversed flow region is about 5-km wide, to its east the model surface winds return to westerly but are not as strong as in the strong downslope flow area just in the lee of the Organ Mountains.

The observed winds are shown by the black arrows. They agree fairly well with the model's wind field with the exception that the observed winds at San Augustine pass are stronger than the model's winds there. The pass is approximately 1 - 2 km wide, so this may be attributable to the model's smoother terrain not adequately resolving the actual San Augustine Pass terrain. We expect that a numerical model will require a horizontal grid spacing of 300 - 400 m or less to adequately resolve the wind flow through the pass.

In Fig. 6, we show the model's surface nonhydrostatic pressure perturbation field compared to the observed pressure perturbations from the ARL and SAMS pressure sensors. The blue dashed lines show the NTU/PU model's forecast of pressure perturbation at the model's surface. The values run from about 0 to -200 pascals (2 hPa) in a band running south to north along the lee side of the Organ Mountains. A little farther east, the model shows a band of little or no perturbation pressure. Even farther east, there is another band of negative perturbation pressure although of somewhat smaller magnitude. These bands continue across the Tularosa basin in connection with the descending parts of the modeled lee waves.

The observations shown include the ARL instrumented towers and the SAMS sites in this area. The observed pressure perturbations were very carefully obtained by interpolation of a given observation's pressure to a common datum plane of 1295 m asl. With the exception of the observation at San Augustine Pass, 1295 m minimized the vertical distance differences with the observation sites. The average vertical distance between this height and the stations' heights was less than 40 m and two of the stations were within 10 m.

There was high thin cloud cover during the morning of 25 January so that surface temperatures rose only a few degrees from the 12 UTC temperatures. The stations' heights were very carefully obtained from GPS and other sources.

Except for San Augustine Pass, the model's values are in good agreement with the observations and support the occurrence of the model's negative pressure perturbation bands. There is also a comparison for the Oro Grande gate SAMS, which is far to the east of this area shown in Fig. 6 where there is a second band of modeled negative perturbation pressure. The observed pressure perturbation at Oro Grande agrees well with the model.

Vertical cross sections of vertical and horizontal wind show bands occur across the Tularosa basin and with the pressure perturbation bands support the occurrence of a hydraulic jump in conjunction with the wind reversal and adverse pressure gradient discussed previously.

Figure 7 shows a west to east cross section of the NTU/PU model vertical velocity at 1500 UTC on 25 January 2004. It is located north of WSMR headquarters approximately intersecting San Augustine Pass and more importantly it intersects the location of the wind profiling radar located at WSMR shown by the dark vertical line. The pattern and magnitude of vertical velocity are comparable to the lee waves observed near the Espinouse Mountains in France on 16 January 1970 (Cruette 1976). The model shows trapped lee waves extending eastward across the Tularosa Basin with maximum vertical velocities greater than 3 m s^{-1}. These were calculated from the El Paso sounding. The theoretical wavelength of about 13 - 14 km was calculated by

$$2\pi V\left[T/g(\gamma_d - \gamma)\right]^{\frac{1}{2}} \quad (4)$$

[American Meteorological Society 2 (AMS2) Glossary, http://glossary.ametsoc.org/wiki/Lee_waves] where V is the wind speed, T the temperature in Kelvins, g is gravity, and γ_d and γ are respectively the dry-adiabatic and ambient lapse rates. The model's wavelength is 14 - 15 km. The observed train waves to the lee of the mountains are consistent with a decrease in height of the Scorer parameter, are well represented by the model's surface winds, and are in agreement with the wind profiler observations.

In addition, in the discussion of trapped waves in A.E. Gills's book (Gill 1982), it is stated that "*the maximum amplitude is obtained when L^{-1} is equal to the resonant wavenumber - a condition nearly satisfied in Scorer's example*." Therefore, we also looked at the width of the mountain barrier shown in Fig. 3 which is about 15 km. The width of the real terrain may be slightly narrower owing to the terrain treatment we used to obtain the same terrain height scale in the model as the real terrain. This needs to be further investigated in future work.

A further comment is that in Scorer's and other papers, there are 2 or 3 different layers in the vertical that are separated by sharp changes in N and U. As mentioned in Hsu and Sun (2001), as sharp changes are not possible in a numerical model, this could affect the modeled wavelength. In future work, the effect on numerical model results of this could be explored by performing very high vertical resolutions, as dz = 75 m used in Sun (2013). Other things to consider are that the model was uniformly initialized with the 12 UTC El Paso sounding. Undoubtedly, the conditions around the

Organ Mountains differed somewhat from this especially for times after 12 UTC.

In Fig. 8, we show a comparison of the model's vertical velocities from 0730 - 0900 local time (1430 - 1600 UTC) on January 25 at the wind profiler location. The y-axis is the height in meters asl while the x-axis is the vertical velocity in m s^{-1}. The model's vertical velocities are shown by continuous color lines; the times are shown in the legend on the upper-right-hand side of this figure. The model shows two peaks in vertical velocity, one maximum is at about 4500 m and the second at about 12000 m. The lower peak's vertical velocities dropped steadily from 0730 - 0800 local time and then level off. The upper peak's vertical velocities are steadier over this time.

The vertical velocities observed by the wind profiler are shown by the black pluses and blue pound signs. These are the mean values for the 0700 - 0800 and 0800 - 0900 time periods, respectively, and what is shown has been smoothed by using a running 5-point mean value because the individual point values are quite noisy. The wind profiler is believed to have an accuracy of 0.5 m s^{-1} so we have added error bars for each observed value. The observations show that the lower maximum's vertical velocities decrease going from hour 1 to hour 2 but the upper maximum's vertical velocities are roughly the same.

4.3 Blocking Effects/Downslope Wind at WSMR 19 January 2004

The domain used is the same as for the preceding case and the model was initialized with the 12 UTC El Paso, Texas, sounding on 19 January 2004, which is shown in Fig. 9.

Because of the variation in terrain heights, some of the areas to the lee of the Organ Mountains on January 19 are subject to blocking while for other areas downslope winds develop. The overall flow situation shown in Fig. 10 is quite complex. The model winds after 3-hr integration are shown by the blue vectors and the observed winds are denoted by the black arrows. While there is blocked flow in the lee of the Organs Mountains, there is also downslope flow on the south side of the Organs and to the north of WSMR post. Both of these areas have lower terrain heights than the central part of the Organ Mountains. Although a conventional measure of whether air will go over or around a terrain obstacle is the Froude number, Sun and Sun (2015) have proved that the Froude number in the traditional mountain meteorology is derived from a flow climbing over a 2D mountain based on Boussinesq fluid, which is not suitable to be applied in the compressible atmosphere because the increase of kinetic energy can come from the decrease of enthalpy (c_p*T) instead of potential energy according to the Bernoulli equation. The Froude number is even more difficult to apply to a 3D mountain, because the flow can split, move around or climb over a 3D mountain. The nonlinear circulation also depends on the stratification, wind, surface friction, as well as the size and detail of the mountain, which is far beyond the scope of linear or weakly nonlinear dynamics. Consequently, further study is required to better understand the complexity of the flow shown in Fig 10. Note that the observations generally confirm the model although the observed winds at San Augustine Pass are somewhat stronger than those given by the model which possibly is due to the inability of 1 km grid point model to adequately resolve a terrain feature like this. The weaker simulated wind over San Augustine Pass may also affect the difference between the simulated wind at grid (111E, 96N) and the observation at that point although the lee-vortex is well reproduced. Another factor could be that the uniform surface roughness used here (z_0 = 10 cm) is less than what the effective surface roughness is over the extremely rugged Organ Mountains terrain. A larger roughness height would tend to increase the boundary layer thickness there reducing the vorticity of the flow around and over the southern part of the mountains. That could affect the model simulation at (111E, 96N). We plan to explore this and other variations from what was used in this report in future work.

4.4 Simulations with Constant Westerly Wind of 5 m s^{-1}

Figure 11 shows that the observed wind pattern on January 25 can be reproduced very well by an initial westerly wind of 5 m s^{-1} with $\Delta x = \Delta y = 2$ km and $\Delta z = 300$ after 4-hr integration. Furthermore, the train of lee waves which has been reported frequently in this area is also revealed clearly in this larger domain simulation. The streamline at z = 1.8 km (Fig. 12) shows vortices on the lee side of each peak. The potential temperature at z = 1.8 km (Fig. 12) shows cold air on both sides of the southern high ridge, which blocks the westerly flow across the high mountain. Hence, the flow on the lee side at z = 1.8 km comes from the reverse flow (from W to E) of the vortex from the lower land. On the other hand, the flow moves across the lower mountains to the north and produces adiabatic cooling on the west and subsidence warming on the lee side at z = 1.8 km. The mountain waves are also clearly shown on the vertical cross section at y = 50 grid in Fig. 13. Those mountain waves and lee vortices are very similar to those that occurred on the lee side of the Central Mountain Range in Taiwan (Sun and Chern 1993). The blocking effects of the WSMR terrain, particularly in the lee of the Organ and San Andres Mountain have been shown in SAMS and other data (Grove and Haines 2002). Grove and Haines noted that the wind flow shown by the SAMS stations was consistent with formation of a lee vortex; however, the number of SAMS stations near the Organ Mountains is limited and additional measurements would be required to fully reveal the actual flow. This was addressed during the 2004 Meso-gamma scale study. The kind of blocking seen in the numerical results also showed up in the observations for

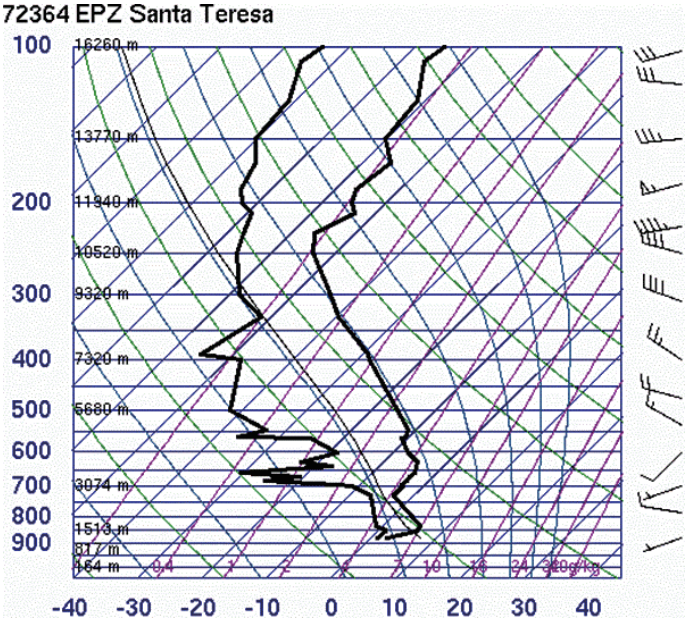

Fig. 9. El Paso, TX, sounding for 19 January 2004, at 12 UTC. Winds below 400 hPa are generally westerly and weak.

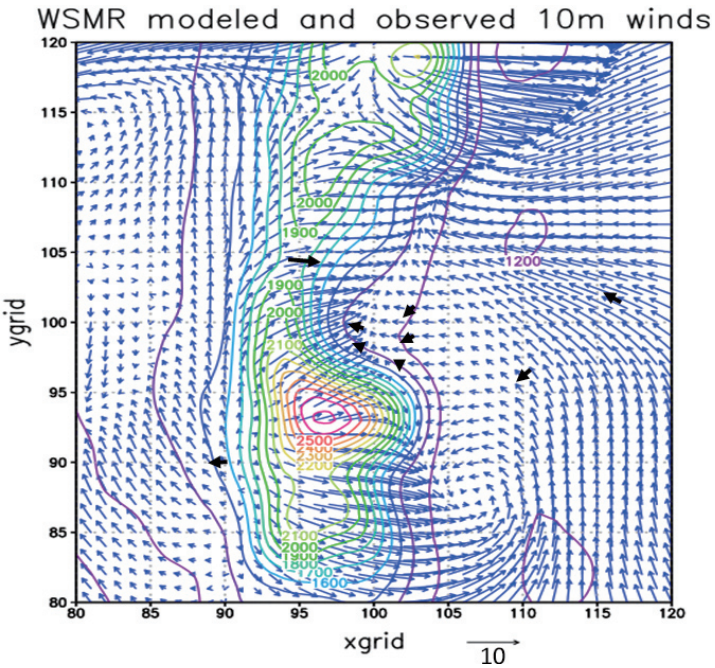

Fig. 10. NTU/PU Surface Wind Field (color vectors) and observed 10 m surface winds (bold black arrows) at 1500 UTC on 19 January 2004.

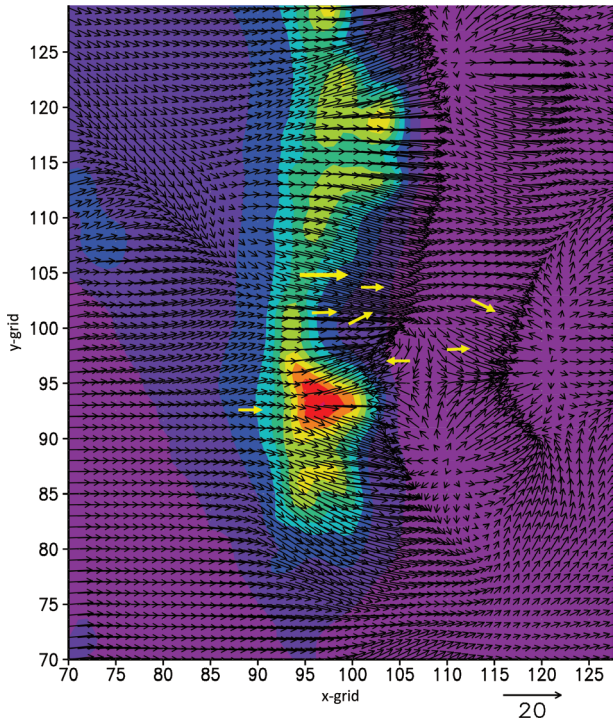

Fig. 11. NTU/PU simulated wind vector at z = 10 m above ground after 4-hr integration from a constant westerly wind of 5 m s^{-1} with $\Delta x = \Delta y = 2$ km and $\Delta z = 300$ m. The observed wind at 1500 UTC 25 January 2004, is indicated by yellow arrow. The arrow at right-lower corner indicates 20 m s^{-1}. The elevation is shaded by color. Yellow arrows are the observed wind at the time.

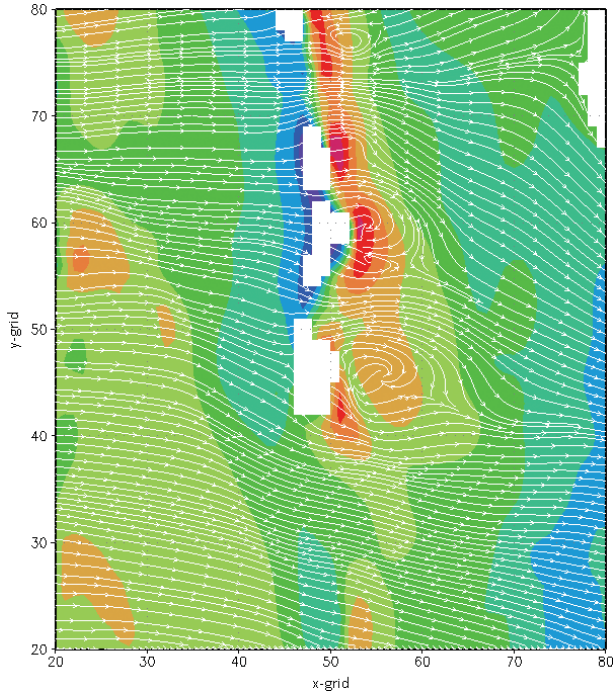

Fig.12. Streamline (white line) and virtual potential temperature (background shaded colors) at z = 1.8 km, warm color (red) indicates subsidence warming on the lee-side, and cold (blue) color adiabatic cooling on the windward side of the mountain. The mountain higher than 1.8 km is indicated by blank.

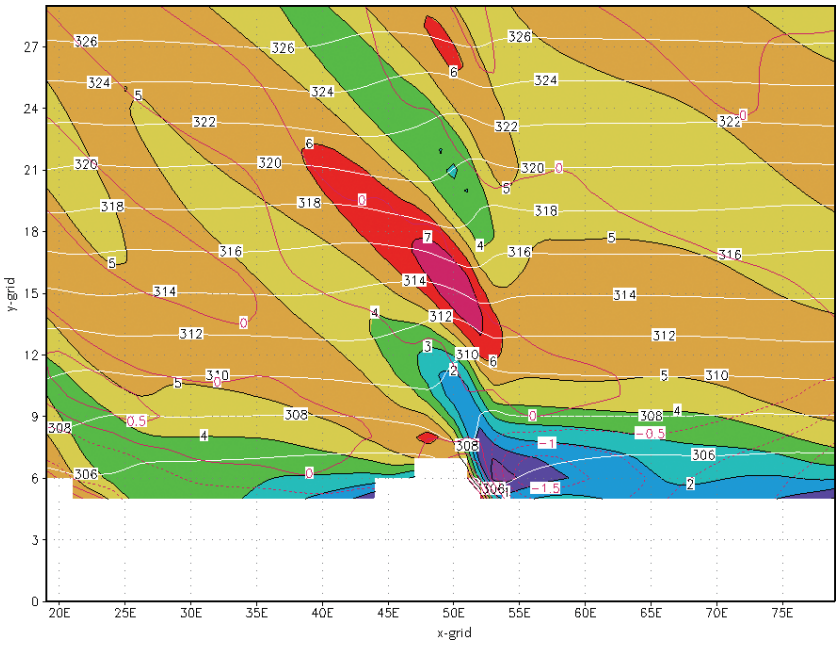

Fig. 13. Vertical cross section of x-component velocity (shaded color and color lines) and potential temperature (white contours) along y = 50 grid in Fig. 12. The initial wind is 5 m s^{-1} coming from west.

westerly and southwesterly flow cases in which the Froude number was less than 0.5. During the January to March 2004 observations, fully and partially blocked flow, lee waves, and hydraulic jumps in the lee of mountains were revealed.

5. CONCLUSIONS

The simulations using the NTU/PU Model over an idealized elliptical mountain and over the Organ Mountains have been presented. For the idealized case, the simulations after 10-hr integration and 20 hr are shown. The model simulation shows a well-defined stagnation point and a wide spread in the transverse direction over the mountain and transit vortices on the lee side.

For the semi-idealized simulations, on 25 January 2004, a downslope wind storm in the lee of these mountains was accompanied by a hydraulic jump, lee waves, and vortices, all of which were well-observed. As shown, the NTU/PU model successfully picks up much of what was observed on this day. For a weak flow imping on the mountains, the model shows that the terrain produces pronounced blocking along with formation of a lee vortex. The model flows are consistent with local WSMR surface flows observed for these kinds of conditions. On 19 January 2004, the WSMR surface observations show over and around the mountain flows. For the case of 19 January the NTU/PU model's wind flow agrees fairly well with the intricacies of the complex flow that was observed.

The skill of the NTU/PU model also depends on the individual case. Therefore, much additional work remains to be done, including improving the numerical scheme, filter, and physics, etc.—especially for the flow over complex terrain. It is also expected that copious data will be collected by the Meteorological Sensor Array (MSA) currently being set up at the Jornada Experimental Range near Las Cruces, New Mexico. The MSA will extend from Jornada over the San Andres Mountains which are a northward extension of the south to north mountain barrier that includes the Organ Mountains. At that particular west to east transect, the mountain barrier is essentially a 1 km high knife edge and will present great challenges for numerical simulation.

Acknowledgements This work was partially supported by the US Army Research Laboratory, the National Science Council, and the National Center for High-performance Computing in Taiwan. Thanks also to Dr. Chris Hocut (ARL) for his review and input on the Introduction and thoughts on the possible impacts a larger roughness length might have on numerical simulations. Finally, thanks to Blaine Thomas of the WSMR flight safety branch for sharing his report on high wind events at WSMR.

REFERENCES

Chen, S. and W. Sun, 2001: Application of the multigrid method and a flexible hybrid coordinate in a nonhydrostatic model. *Mon. Weather Rev.*, **129**, 2660-2676, doi: 10.1175/1520-0493(2001)129<2660:AOTMMA>2.0.CO;2. [Link]

Chern, J. D., 1989: Numerical simulation of stratified flow

past an isolated mountain and lee cyclogenesis. Master Thesis, Department of Earth and Atmospheric Sciences, Purdue University, 85 pp.

Cruette, D., 1976: Experimental study of mountain lee-waves by means of satellite photographs and aircraft measurements. *Tellus*, **28**, 499-523, doi: 10.3402/tellusa.v28i6.11318. [Link]

Deardorff, J. W., 1980: Stratocumulus-capped mixed layers derived from a three-dimensional Model. *Bound.-Layer Meteor.*, **18**, 495-527, doi: 10.1007/bf00119502. [Link]

Doyle, J. D., D. R. Durran, C. Chen, B. A. Colle, M. Georgelin, V. Grubisic, W. R. Hsu, C. Y. Huang, D. Landau, Y. L. Lin, G. S. Poulos, W. Y. Sun, D. B. Weber, M. G. Wurtele, and M. Xue, 2000: An intercomparison of model-predicted wave breaking for the 11 January 1972 Boulder windstorm. *Mon. Weather Rev.*, **128**, 901-914, doi: 10.1175/1520-0493(2000)128<0901:AIOMPW>2.0.CO;2. [Link]

Durran, D. R., 2003: Lee Waves and Mountain Waves. In: Holton, J. R. (Ed.), Encyclopedia of Atmospheric Sciences, Academic Press, 1161-1169, doi: 10.1016/B0-12-227090-8/00202-5. [Link]

Fernando, H. J., E. R. Pardyjak, S. Di Sabatino, F. K. Chow, S. F. De Wekker, S. W. Hoch, J. Hacker, J. C. Pace, T. Pratt, Z. Pu, W. J. Steenburgh, C. D. Whiteman, Y. Wang, D. Zajic, B. Balsley, R. Dimitrova, G. D. Emmitt, C. W. Higgins, J. C. Hunt, J. C. Knievel, D. Lawrence, Y. Liu, D. F. Nadeau, E. Kit, B. W. Blomquist, P. Conry, R. S. Coppersmith, E. Creegan, M. Felton, A. Grachev, N. Gunawardena, C. Hang, C. M. Hocut, G. Huynh, M. E. Jeglum, D. Jensen, V. Kulandaivelu, M. Lehner, L. S. Leo, D. Liberzon, J. D. Massey, K. McEnerney, S. Pal, T. Price, M. Sghiatti, Z. Silver, M. Thompson, H. Zhang, and T. Zsedrovits, 2015: The MATERHORN: Unraveling the Intricacies of Mountain Weather. *Bull. Amer. Meteorol. Soc.*, **96**, 1945-1967, doi: 10.1175/BAMS-D-13-00131.1. [Link]

Fernando, H. J. S., J. Mann, J. M. L. M. Palma, J. K. Lundquist, R. J. Barthelmie, M. BeloPereira, W. O. J. Brown, F. K. Chow, T. Gerz, C. M. Hocut, P. M. Klein, L. S. Leo, J. C. Matos, S. P. Oncley, S. C. Pryor, L. Bariteau, T. M. Bell, N. Bodini, M. B. Carney, M. S. Courtney, E. D. Creegan, R. Dimitrova, S. Gomes, M. Hagen, J. O. Hyde, S. Kigle, R. Krishnamurthy, J. C. Lopes, L. Mazzaro, J. M. T. Neher, R. Menke, P. Murphy, L. Oswald, S. Otarola-Bustos, A. K. Pattantyus, C. Veiga Rodrigues, A. Schady, N. Sirin, S. Spuler, E. Svensson, J. Tomaszewski, D. D. Turner, L. van Veen, N. Vasiljević, D. Vassallo, S. Voss, N. Wildmann, and Y. Wang, 2018: The Perdigão: Peering into Microscale Details of Mountain Winds. *Bull. Amer. Meteorol. Soc.*, doi: 10.1175/bams-d-17-0227.1. [Link]

Gill, A. E., 1982: Atmosphere-Ocean Dynamics, Academic Press, 662 pp.

Grove, D. J. and P. A. Haines, 2002: Fine scale numerical prediction of atmospheric flow in complex terrain. 2002 DRI Report, US Army Research Laboratory, Adelphi, MD.

Grubišić, V., J. D. Doyle, J. Kuettner, S. Mobbs, R. B. Smith, C. D. Whiteman, R. Dirks, S. Czyzyk, S. A. Cohn, S. Vosper, M. Weissmann, S. Haimov, S. F. J. De Wekker, L. L. Pan, and F. K. Chow, 2008: THE TERRAIN-INDUCED ROTOR EXPERIMENT: A Field Campaign Overview Including Observational Highlights. *Bull. Amer. Meteorol. Soc.*, **89**, 1513-1534, doi: 10.1175/2008BAMS2487.1. [Link]

Haines, P. A., J. D. Chern, and W. Y. Sun, 1997: Numerical simulation of the Valentine's Day storm during the 1990 winter icing and storms project. *Tellus A*, **49**, 595-612, doi: 10.1034/j.1600-0870.1997.t01-4-00006.x. [Link]

Haines, P. A., D. J. Grove, W. Y. Sun, W.-R. Hsu, and S. C. Tcheng, 2003: High resolution results and scalability of numerical modeling of wind flow at White Sands Missile Range. BACIMO (DOD atmospheric science and effects) Conference, September 2003 in Monterey, California.

Haines, P. A., D. J. Grove, W. Y. Sun, and W. R. Hsu, 2006: Observations and Numerical Modeling of Sub and Super-critical Flow at White Sands Missile Range. 12th Conference on Mountain Meteorology, the American Meteorological Society, Santa Fe, NM.

Hsu, W. R. and W. Y. Sun, 2001: A time-split, forward-backward numerical model for solving a nonhydrostatic and compressible system of equations. *Tellus A*, **53**, 279-299, doi: 10.3402/tellusa.v53i3.12195. [Link]

Hsu, W. R., M. E. Shieh, and W. Y. Sun, 2006: Simulations of mountain waves and lee vortices using an explicit, semi- Lagrangian numerical model. 12th Mountain Meteorology Conference, the American Meteorological Society, Santa Fe, NM.

Hunt, J. C. R., K. J. Richards, and P. W. M. Brighton, 1988: Stably stratified shear flow over low hills. *Q. J. R. Meteorol. Soc.*, **114**, 859-886, doi: 10.1002/qj.49711448203. [Link]

Mobbs, S. D., S. B. Vosper, P. F. Sheridan, R. Cardoso, R. R. Burton, S. J. Arnold, M. K. Hill, V. Horlacher, and A. M. Gadian, 2005: Observations of downslope winds and rotors in the Falkland Islands. *Q. J. R. Meteorol. Soc.*, **131**, 329-351, doi: 10.1256/qj.04.51. [Link]

Sheridan, P. F., V. Horlacher, G. G. Rooney, P. Hignett, S. D. Mobbs, and S. B. Vosper, 2007: Influence of lee waves on the near-surface flow downwind of the Pennines. *Q. J. R. Meteorol. Soc.*, **133**, 1353-1369, doi: 10.1002/qj.110. [Link]

Shieh, M. E., W. R. Hsu, and W. Y. Sun, 2006: Applications of a monotone semi-Lagrangian advection scheme on

a 3D nonhydrostatic model and squall line simulations. Computational Fluid Dynamics Conference, Wan-Li, Taiwan.

Shieh, M. E., W. R. Hsu, and W. Y. Sun, 2011: Applications of a three-dimensional nonhydrostatic atmospheric model on uniform flows over an idealized mountain. 2010 CFD Taiwan Jhongi, Taiwan.

Smith, R. B., 1979: The influence of mountains on the atmosphere. In: Saltzman, B. (Ed.), Advances in Geophysics, Vol. 21, Academic Press, 87-230, doi: 10.1016/S0065-2687(08)60262-9. [Link]

Smith, R. B. and S. Grønås, 1993: Stagnation points and bifurcation in 3-D mountain airflow. *Tellus A*, **45**, 28-43, doi: 10.3402/tellusa.v45i1.14840. [Link]

Sun, W. Y., 1993: Numerical experiments for advection equation. *J. Comput. Phys.*, **108**, 264-271, doi: 10.1006/jcph.1993.1181. [Link]

Sun, W. Y., 2011: Instability in leapfrog and forward–backward schemes: Part II: Numerical simulations of dam break. *Comput. Fluids*, **45**, 70-76, doi: 10.1016/j.compfluid.2010.11.002. [Link]

Sun, W. Y., 2013: Numerical study of severe downslope windstorm. *Weather and Climate Extremes*, **2**, 22-30, doi: 10.1016/j.wace.2013.10.002. [Link]

Sun, W. Y., 2016: The vortex moving toward Taiwan and the influence of the Central Mountain Range. *Geosci. Lett.*, **3**, doi: 10.1186/s40562-016-0052-5. [Link]

Sun, W. Y. and C. Z. Chang, 1986: Diffusion model for a convective layer. Part I: Numerical simulation of convective boundary layer. *J. Clim. Appl. Meteorol.*, **25**, 1445-1453, doi: 10.1175/1520-0450(1986)025<1445:DMFACL>2.0.CO;2. [Link]

Sun, W. Y. and J. D. Chern, 1993: Diurnal variation of lee vortices in Taiwan and the surrounding area. *J. Atmos. Sci.*, **50**, 3404-3430, doi: 10.1175/1520-0469(1993)050<3404:DVOLVI>2.0.CO;2. [Link]

Sun, W. Y. and J. D. Chern, 1994: Numerical experiments of vortices in the wakes of large idealized mountains. *J. Atmos. Sci.*, **51**, 191-209, doi: 10.1175/1520-0469(1994)051<0191:NEOVIT>2.0.CO;2. [Link]

Sun, W. Y. and W. R. Hsu, 2005: The effects of surface friction on downslope wind and mountain waves. *Terr. Atmos. Ocean. Sci.*, **16**, 393-418, doi: 10.3319/TAO.2005.16.2.393(A). [Link]

Sun, W. Y. and O. M. Sun, 2013: Numerical simulation of Rossby wave in shallow water. *Comput. Fluids*, **76**, 116-127, doi: 10.1016/j.compfluid.2013.01.018. [Link]

Sun, W. Y. and O. M. Sun, 2015: Bernoulli equation and flow over a mountain. *Geosci. Lett.*, **2**, doi: 10.1186/s40562-015-0024-1. [Link]

Sun, W. Y., J. D. Chern, C. C. Wu, and W. R. Hsu, 1991: Numerical simulation of mesoscale circulation in Taiwan and surrounding area. *Mon. Weather Rev.*, **119**, 2558-2573, doi: 10.1175/1520-0493(1991)119<2558:nsomci>2.0.co;2. [Link]

Sun, W. Y., W. R. Hsu, J. D. Chern, S. H. Chen, C. C. Wu, K. J.-S. Yang, K. Yeh, M. G. Bosilovich, P. A. Haines, K. H. Min, T. J. Oh, B. T. MacCall, A. Yildirim, Y. L. Chang, C. Z. Chang, and Y. C. Yu, 2008: Purdue atmospheric models and applications. In: Liao, K. N. and M. D. Chou (Eds.), Recent Progress in Atmospheric Sciences: Applications to the Asia-Pacific Region, World Scientific, Singapore, 200-228, doi: 10.1142/9789812818911_0012. [Link]

Sun, W. Y., O. M. Sun, and K. Tsuboki, 2012: A modified atmospheric non-hydrostatic model on low aspect ratio grids. *Tellus A*, **64**, doi: 10.3402/tellusa.v64i0.17516. [Link]

Sun, W. Y., O. M. Sun, and K. Tsuboki, 2013: A modified atmospheric non-hydrostatic model on low aspect ratio grids: Part II. *Tellus A*, **65**, doi: 10.3402/tellusa.v65i0.19681. [Link]

Takacs, L. L., 1985: A two-step scheme for the advection equation with minimized dissipation and dispersion errors. *Mon. Weather Rev.*, **113**, 1050-1065, doi: 10.1175/1520-0493(1985)113<1050:ATSSFT>2.0.CO;2. [Link]

Thomas, B., 2014: A Statistical Model for High Wind Event Forecasting at White Sands Main Post and San Augustin Pass Internal White Paper, Flight Safety Branch, U.S. Army White Sands Missile Range, White Sands Missile Range, New Mexico.

Wen, C. Y. and C. Y. Lin, 2001: Two-dimensional vortex shedding of a circular cylinder. *Phys. Fluid.*, **13**, 557-560, doi: 10.1063/1.1338544. [Link]

Whiteman, C. D., A. Muschinski, S. Zhong, D. Fritts, S. W. Hoch, M. Hahnenberger, W. Yao, V. Hohreiter, M. Behn, Y. Cheon, C. B. Clements, T. W. Horst, W. O. J. Brown, and S. P. Oncley, 2008: METCRAX 2006: Meteorological experiments in Arizona's Meteor Crater. *Bull. Amer. Meteorol. Soc.*, **89**, 1665-1680, doi: 10.1175/2008BAMS2574.1. [Link]